Article

Cite This: *Biomacromolecules* 2018, 19, 1614−1624

pubs.acs.org/Biomac

# Engineered Coiled-Coil Protein for Delivery of Inverse Agonist for Osteoarthritis

Liming Yin,[†] Albert S. Agustinus,[†] Carlo Yuvienco,[†] Takeshi Minashima,[‡] Nicole L. Schnabel,[†] Thorsten Kirsch,*[,‡] and Jin K. Montclare*[,†,§,∥,⊥,#]

[†]Department of Chemical and Biomolecular Engineering, NYU Tandon School of Engineering, Brooklyn, New York 11201, United States

[‡]Department of Orthopaedic Surgery and [§]Department of Radiology, NYU School of Medicine, New York, New York 10010, United States

[∥]Department of Chemistry, New York University, New York, New York 10003, United States

[⊥]Department of Biomaterials, NYU College of Dentistry, New York, New York 10010, United States

[#]Department of Biochemistry, SUNY Downstate Medical Center, Brooklyn, New York 11203, United States

Supporting Information

**ABSTRACT:** Osteoarthritis (OA) results from degenerative and abnormal function of joints, with localized biochemistry playing a critical role in its onset and progression. As high levels of *all-trans* retinoic acid (ATRA) in synovial fluid have been identified as a contributive factor to OA, the synthesis of *de novo* antagonists for retinoic acid receptors (RARs) has been exploited to interrupt the mechanism of ATRA action. BMS493, a pan-RAR inverse agonist, has been reported as an effective inhibitor of ATRA signaling pathway; however, it is unstable and rapidly degrades under physiological conditions. We employed an engineered cartilage oligomeric matrix protein coiled-coil ($C_{cc}^{S}$) protein for the encapsulation, protection, and delivery of BMS493. In this study, we determine the binding affinity of $C_{cc}^{S}$ to BMS493 and the stimulator, ATRA, via competitive binding assay, in which ATRA exhibits approximately 5-fold superior association with $C_{cc}^{S}$ than BMS493. Interrogation of the structure of $C_{cc}^{S}$ indicates that ATRA causes about 10% loss in helicity, while BMS493 did not impact the structure. Furthermore, $C_{cc}^{S}$ self-assembles into nanofibers when bound to BMS493 or ATRA as expected, displaying 11−15 nm in diameter. Treatment of human articular chondrocytes *in vitro* reveals that $C_{cc}^{S}$·BMS493 demonstrates a marked improvement in efficacy in reducing the mRNA levels of matrix metalloproteinase-13 (MMP-13), one of the main proteases responsible for the degradation of the extracellular cartilage matrix compared to BMS493 alone in the presence of ATRA, interleukin-1 beta (IL-1$\beta$), or IL-1 $\beta$ together with ATRA. These results support the feasibility of utilizing coiled-coil proteins as drug delivery vehicles for compounds of relatively limited bioavailability for the potential treatment of OA.

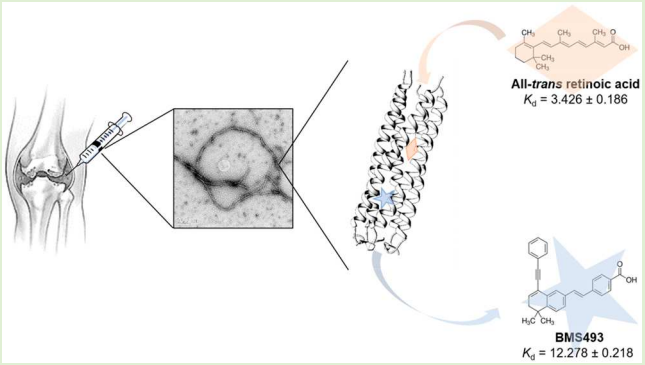


## INTRODUCTION

Osteoarthritis (OA) involves joint degeneration and prevents the joint structure from normal function; it has been recognized as a prevalent chronic disease, contributing to the aging population,[1] traumatic injury,[2] and epidemic of obesity.[3] OA is characterized by a failure of tissue homeostasis between synthesis and degradation of extracellular matrix (ECM) components such as collagen[4] and proteoglycan[5] with a net loss, and several proteases have been reported to involve in ECM destruction, including a disintegrin and metalloproteinase with thrombospondin type 1 motif 5 (ADAMTS5) and matrix metalloproteinase 13 (MMP-13).[6] Resident chondrocytes transition to hypertrophic phenotype from articular phenotype,[7,8] and this phenotypic change as well as the execution of terminal differentiation events has been established to associate with OA progression.[9−13]

*all-trans*-Retinoic acid (ATRA), a derivative of vitamin A, which is well-documented to regulate cartilage and skeleton formation has been identified as a potent inducer of hypertrophic phenotype, stimulating the expression of matrix metalloproteinases and aggrecanases that are responsible for the degradation of ECM.[13,14] Thus, OA and its progression have been attributed to high levels of ATRA in synovial fluid. ATRA and the precursory retinoids signal through retinoic acid receptors (RARs), which belong to the nuclear receptor

**Received:** January 31, 2018
**Revised:** March 29, 2018
**Published:** March 30, 2018






DOI: 10.1021/acs.biomac.8b00158
*Biomacromolecules* 2018, 19, 1614−1624

superfamily of transcription factors and contribute to a variety of physiological processes.[15] Under this superfamily, RARs and rexinoid receptors (RXRs) consist of three members: $\alpha$, $\beta$, and $\gamma$.[16] While chondrocytes mainly express RAR$\alpha$ and RAR$\gamma$,[17] ATRA activates all three species[16] that form heterodimers with RXR (RAR-RXR) and act as ligand-dependent transcription factors binding to specific response elements within the promoters of target genes when complexed with a number of coregulators.[18,19] The small hydrophobic molecule, BMS493 (((*E*))4-[2-[5,5-dimethyl-8-(2-phenylethynyl)-5,6-dihydronaphthalen-2-yl]ethen-1-yl]benzoic acid), is a potent pan-RAR inverse agonist that stabilizes the interaction between RAR-RXR heterodimer and nuclear corepressor,[19−21] exhibiting high resistance to ECM degradation and potential as an OA therapeutic. However, BMS493 is light sensitive, readily degrading, and/or isomerizing to ineffective products.

Currently, synthetic polymers, including liposomes,[22] micelles,[23] and polymers,[24,25] have been at the forefront in drug delivery. Because of disadvantages of certain synthetic polymers, e.g., pro-inflammatory[26,27] and pro-immunogenic[28] activities as well as difficulties with regulatory authorities in clinical trials,[29] there are no polymeric drug delivery system for administration in humans currently registered for the treatment of rheumatic diseases.[30] As an alternative, we have explored the use of engineered proteins[31] as a biocompatible delivery agent to carry and protect the small molecule BMS493.

Coiled-coil proteins have been extensively studied and developed for a variety of biomedical applications, such as tissue engineering, biosensor, and therapeutic delivery.[32−39] Eriksson et al. have demonstrated that right-handed coiled-coil (RHCC) can carry the platinum-containing chemotherapeutic drug cisplatin. The complex has been observed to internalize into the human cell line FaDu cells from a hypopharyngeal carcinoma in an *in vivo* study.[35] *In vitro*, cisplatin incorporated in RHCC exhibits retained and enhanced cytotoxicity against various tumor cell lines than cisplatin alone.[35] On the basis of the coiled-coil motif of human matrilin-1 near C-terminus, Fan et al. have fabricated the amphiphilic peptide P45, applying the hydrophobic helix domain for self-assembly, a negatively charged sequence (Glu-Glu-Asp) to interact with the chemotherapy drug doxorubicin, and the additional RGD peptide (Arg-Gly-Asp) to target A549 cells from human lung carcinoma.[36] Triggered by doxorubicin, the P45 self-assembles into ∼60 nm spherical nanoparticles and exhibits comparable $IC_{50}$ values as well as higher cytotoxicity level to $\alpha_v\beta_3$-expressing cell line.[36] Through further modification of coiled-coils, Ding et al. have employed two complementary peptides to cross-link hyaluronic acid nanogels with approximately 170 nm in diameter, in which saporin (SAP), a ribosome inactivating protein, is loaded.[37] When uptaken by MCF-7 cancer cells, the uncoiling of the peptides is triggered by the acidic condition in the cytoplasm to release SAP, resulting in significantly enhanced apoptotic activity with an $IC_{50}$ at 12.2 nM, whereas free SAP exhibits limited antitumor activity at the same concentration.[37] Pechar et al. have formulated a *N*-(2-hydroxypropyl)methacrylamide (HPMA) backbone bearing pirarubicin and a coiled-coil that could heterodimerize with the another helix carrying a single-chain fragment derived from a B1 monoclonal antibody.[38] In an *in vivo* study, the targeting conjugate prolongs the median survival time of BCL1 leukemia mice by 24 days more than the administration of free pirarubicin.[38] Recently, Wu et al. have developed a coiled-coil pair in which one is linked to HPMA-based copolymer and the other to an antigen-binding fragment that targets B lymphocytes; the coiled-coils attached to the HPMA-based copolymer trigger the cross-linking of CD20 and consequently lead to apoptosis, resulting in a drug-free therapy for non-Hodgkin's lymphoma.[39] While these designed coiled-coil proteins and conjugates facilitate the delivery of chemotherapeutics, herein we focus on the delivery of BMS493 and treatment of OA.

Our group has been engineering protein biomaterials composed of cartilage oligomeric matrix protein coiled-coil ($C_{cc}$) in which the cysteines are replaced with serines ($C_{cc}^{S}$),[40,41] modified coiled-coils,[42−44] and fusions with elastin sequence motifs.[45−49] Cartilage oligomeric matrix protein (COMP) is a 524 kDa noncollagenous extracellular matrix glycoprotein found in cartilage, tendon, and ligament.[50−53] As a member in the thrombospondin family,[51] COMP consists of 5 homogeneous monomers oligomerized at the N-terminus via the coiled-coil structure stabilized by disulfide bridges. Following the $C_{cc}$ domain, each monomer is composed of 4 epidermal growth factor motifs, 8 thrombospondin type 3 repeats, and a globular C-terminus.[54,55] $C_{cc}$ is approximately 6.9 kDa and capable of self-assembling into a homopentamer with a hydrophobic core that is 7.3 nm in length and 0.2−0.6 nm in diameter,[56−59] suggesting that its role is to store 1,25-dihydroxy-vitamin D3 or ATRA for signaling events during cartilage morphogenesis and therefore suitable as a delivery vehicle in OA treatment. $C_{cc}$ and $C_{cc}^{S}$ can accommodate several other ligands including curcumin (CCM), *all-trans*-retinal (ATR, vitamin A), and a range of fatty acids.[41,59,60]

CCM, a principal bioactive component of *Curcuma longa* (tumeric), has been recognized as a potent chemopreventive with numerous advantages, including antioxidative and anti-inflammatory properties.[61,62] Despite its high pharmaceutical value, CCM exhibits low solubility and thus limited bioavailability; thus, researchers have been developing delivery systems to advance the efficacy.[63] As reported in the literature,[41,42,47] we have been utilizing CCM as a model therapeutic to evaluate $C_{cc}^{S}$-based delivery agents since it exhibits fluorescence upon binding to the protein. Furthermore, we have previously identified several residues throughout the hydrophobic pore, including L37, L44, V47, and L51 near the N-terminus and Q54, V65, and S68 near the C-terminal region of $C_{cc}^{S}$ crucial for structure, stability, assembly, and small molecule binding.[41] Because of the traceability via fluorescence, CCM is introduced in competitive assays to investigate the binding of BMS493 and ATRA to $C_{cc}^{S}$ for potential treatment of OA. Our studies demonstrate that the structural conformation and fiber morphology of BMS493 bound $C_{cc}^{S}$ is preserved. Moreover, the affinity of BMS493 toward $C_{cc}^{S}$ is 5-fold lower than ATRA, serving as a driving force to release BMS493 from the $C_{cc}^{S}$·BMS493 complex. In the presence of ATRA, the $C_{cc}^{S}$·BMS493 complex exhibits at least 11.5% higher efficacy than free BMS493 treated *in vitro* to chondrocytes.

## EXPERIMENTAL SECTION

**Materials.** Curcumin (CCM) and *all-trans*-retinoic acid (ATRA) were obtained from Acros while BMS493 was purchased from Santa Cruz. Uranyl acetate was attained from Electron Microscopy Sciences and 30% acrylamide/bis solution from Bio-Rad. Tryptic soy agar, tryptone, sodium chloride, calcium chloride, manganese chloride, cobalt chloride, zinc sulfate, copper chloride, nickel chloride, sodium selenite, boric acid, sodium molybdate, iron(III) chloride, magnesium



DOI: 10.1021/acs.biomac.8b00158
*Biomacromolecules* 2018, 19, 1614−1624

sulfate, 20 essential amino acids, glucose, glycerol, lactose, thiamine hydrochloride, ampicillin, monopotassium phosphate, monosodium phosphate, disodium phosphate, sodium dodecyl sulfate, Tris base, urea, imidazole, tricine, dithiothreitol, ammonium chloride, ammonium persulfate, tetramethylethylenediamine, Coomassie brilliant blue, methanol, ethanol (EtOH), acetic acid, and hydrochloride were acquired from Fisher Scientific. All reagents for protein production were filtered with 0.22 $\mu$m filters (EMD Millpore) prior to the usage. Both the 1 mL HiTrap IMAC FastFlow column and 5 mL desalting columns were purchased from GE Life Sciences. The Hellma absorption cuvette was acquired from Sigma-Aldrich. The 96-well solid black polystyrene microplates were obtained from Corning. Micro BCA protein assay kit, endotoxin removal columns, and *Limulus* amebocyte lysate (LAL) chromogenic quantitation kit were purchased from Thermo Fisher Scientific. Formvar/carbon-coated 400 mesh copper grids were procured from Electron Microscopy Sciences. Dulbecco's modified Eagle's medium (DMEM) was acquired from Life Technologies. Fetal calf serum (FCS) was purchased from HyClone. L-Glutamine, penicillin, and streptomycin were procured from Invitrogen. RNeasy Minikit and Omniscript RT Kit were purchased from Qiagen. The SYBR Green PCR Master Mix Kit was acquired from Applied Biosystems.

**Protein Production.** pQE9/COMPcc$^{S41}$ was transformed into *E. coli* strain BL21(DE3), and a single colony was inoculated into 10 mL of 1X M9 minimal medium supplemented with 0.02% v/v trace metal mixture (consisting of 20 mM $CaCl_2$, 10 mM $MnCl_2$, 2 mM $CoCl_2$, 10 mM $ZnSO_4$, 2 mM $CuCl_2$, 2 mM $NiCl_2$, 2 mM $Na_2SeO_3$, 2 mM $H_3BO_3$, 2 mM $Na_2MoO_4$, 50 mM $FeCl_3$[64]), 100 $\mu$g/mL 20 amino acids, 0.4% w/v glucose, 0.1 mM $CaCl_2$, 1 mM $MgSO_4$, 35 $\mu$g/mL thiamine hydrochloride, 200 $\mu$g/mL ampicillin, and incubated at 37 °C overnight shaking at 350 rpm. The starter culture was subcultured 4% v/v in a 200 mL autoinduction media in which 1X M9 was supplemented with 0.02% v/v trace metal mixture, 100 $\mu$g/mL 20 amino acids, 0.1 mM $CaCl_2$, 1 mM $MgSO_4$, 35 $\mu$g/mL thiamine hydrochloride, 200 $\mu$g/mL ampicillin, 0.5% w/v glycerol, 0.05% w/v glucose, 0.2% w/v lactose,[64] and incubated for 8 h at 37 °C shaking at 350 rpm. Cells were harvested by centrifugation at 5000 rpm at 4 °C for 30 min on Allegra 25R Centrifuge (Beckman Coulter) and stored at −20 °C prior to purification. The protein expression was confirmed by sodium dodecyl sulfate−polyacrylamide gel electrophoresis (SDS-PAGE).

The cell pellet was resuspended in buffer containing 50 mM $Na_2HPO_4$ and 6 M urea at pH 8.0, followed by two cycles of freezing and thawing and then lysis on ice via Q500 Sonicator (Qsonica) with 75% amplitude for 3 min. After centrifugation at 14 000 rpm at 4 °C for 2 h, the lysate was obtained and applied to a 1 mL $CoCl_2$-charged HiTrap IMAC FastFlow column installed on the ÄKTA Purifier System (GE Life Sciences) at 4 °C. Proteins were eluted with buffer consisting of 50 mM $Na_2HPO_4$, 6 M urea, and 500 mM imidazole, pH 8.0. Upon the examination of purity via SDS-PAGE (Figure S1), the elutions were desalted using a 5 mL Sephadex G-25 loaded HiTrap desalting column against 100 mM Gomori phosphate buffer, pH 8.0, which was performed on the ÄKTA Purifier System at 4 °C. Concentration of purified $C_{cc}$ protein was determined by the Micro BCA protein assay kit ranging from 130 to 220 $\mu$M in approximately 2.5 mL, resulting in 1.0−1.5 mg/mL.

**Endotoxin Removal.** Purified $C_{cc}^S$ was isolated from pyrogenic lipopolysaccharides with an endotoxin removal column containing porous cellulose beads modified by poly($\varepsilon$-lysine). All reagents were freshly prepared with pyrogen-free water (EMD Millipore) and filtered through sterile 0.22 $\mu$m filters. Approximately 50% v/v protein was loaded onto the column containing 1 mL of endotoxin removal resin, followed by incubation on a rotator (Barnstead Thermolyne) at room temperature for an hour prior to elution. An additional 1 mL of 100 mM Gomori phosphate buffer pH 8.0 was introduced as a wash step and collected. Both elution and wash were assessed for residual endotoxin by the commercially available LAL chromogenic quantitation kit.

**Circular Dichroism (CD) Spectroscopy.** Samples of approximately 10 $\mu$M $C_{cc}^S$ in the absence and presence of 20 $\mu$M CCM, 50 $\mu$M BMS493, 50 $\mu$M ATRA, 20 $\mu$M CCM + 50 $\mu$M BMS493, 20 $\mu$M CCM + 50 $\mu$M ATRA, and 50 $\mu$M BMS493 + 50 $\mu$M ATRA in 100 mM Gomori phosphate buffer, pH 8.0, containing 10% v/v EtOH were incubated at 25 °C shaking at 300 rpm on a Thermomixer R (Eppendorf) for 2 h in the dark. The samples were loaded into a 1 mm quartz cuvette and analyzed for secondary structure on a J-815 circular dichroism polarimeter (Jasco). Wavelength scans were performed at 25 °C from 260 to 190 nm with a 1 nm step size. Temperature scans were accomplished by monitoring signals at 222 nm from 25 to 75 °C at a heating rate of 1 °C/min. All scans were collected as averages of three consecutive spectra and subtracted from the background of 100 mM Gomori phosphate buffer pH 8.0 in the presence or absence of 10% v/v EtOH or small molecules.

Mean residue ellipticity (MRE), $[\theta]_{MRE}$, was converted from the observed ellipticity signal, $[\theta]_{obs}$, and calculated by applying the equation $[\theta]_{MRE} = [\theta]_{obs}/(10 \times c \cdot p \cdot l)$, where $c$ is molar concentration of $C_{cc}^S$, $p$ is the path length of the cell in centimeter, and $l$ is the number of amino acids.[65] Melting temperature ($T_m$) of $C_{cc}^S$ was determined by calculating the first derivative of fraction folded ($F$) curve, which was analyzed with the equation $F = ([\theta]_{MRE} - \theta_U)/(\theta_N - \theta_U)$, where $\theta_U$ and $\theta_N$ are the $[\theta]_{MRE}$ at 222 nm ($\theta_{222\ nm}$)[66] from 25 to 75 °C of completely unfolded and folded protein, respectively. The temperature of $C_{cc}^S$ $_c$ undergoing the refolding ($T_r$) was determined with the same equation. Helical content was calculated using the expression $100 \times [\theta_{222\ nm}/(\theta_{max})_{222\ nm}]$, where $(\theta_{max})_{222\ nm} = -40000 \times [1 - (2.5/n)]$ ($n = 61$).[41,67] The Gibbs free energy of folding was solved with the equation $\Delta G° = -RT \ln K = \Delta H° - T\Delta S°$, where $R$ is the gas constant $1.987 \times 10^{-3}$, $T$ is the absolute temperature at 25 °C (298 K), $K$ is equal to $F/(1 - F)$, and $\Delta H°$ and $\Delta S°$ represent the standard enthalpy and entropy change at $T_m$ (K), respectively. All data represent averages of three independent trails of $C_{cc}^S$.

**Competition Binding Assay.** Approximately 10 $\mu$M $C_{cc}^S$ was incubated with 0−30 $\mu$M CCM in 100 mM Gomori phosphate buffer, pH 8.0, containing 10% v/v EtOH at 25 °C shaking at 300 rpm on a Thermomixer R (Eppendorf) for 2 h in the dark. The dissociation constant ($K_d$) of $C_{cc}^S$ for CCM was determined by recording the fluorescence emission at 490 nm upon excitation at 420 nm on a Synergy H1 microplate reader (BioTek). For the competition binding, 10 $\mu$M $C_{cc}^S$ with 15 $\mu$M CCM was mixed with 0 to 50 $\mu$M BMS493 or 0 to 150 $\mu$M ATRA, respectively, in 200 $\mu$L of 100 mM Gomori phosphate buffer, pH 8.0, containing 10% v/v EtOH and incubated for 2 h at room temperature shaking at 300 rpm on a Thermomixer R (Eppendorf) in the dark. Fluorescence of CCM was then measured as described above. Each study were averaged from triplicates and subtracted from the background of the respective small molecule in 100 mM Gomori phosphate buffer, pH 8.0, with 10% v/v EtOH prior to analysis with GraphPad Prism (GraphPad Software). The binding studies of CCM were analyzed with the equation $y = B_{max} \cdot x/(K_d + x)$, where $B_{max}$ is the maximum binding in the same unit as $y$; competition binding assays were processed with the equations $y$ = bottom + (top − bottom)/$(1 + 10^{x - \log EC_{50}})$ and $\log EC_{50} = \log(10^{\log K_i(1+[CCM]/K_d\ of\ CCM)})$, where top and bottom are the highest and lowest intensity in the competition binding curves, respectively, and $K_i$ represents the dissociation constant of BMS493 or ATRA. All data represent averages of three independent studies of $C_{cc}^S$.

**Morphological Studies via Transmission Electron Microscopy (TEM).** The following samples of 10 $\mu$M $C_{cc}^S$ in the absence and presence of 20 $\mu$M CCM, 50 $\mu$M BMS493, 50 $\mu$M ATRA, 20 $\mu$M CCM + 50 $\mu$M BMS493, 20 $\mu$M CCM + 50 $\mu$M ATRA, and 50 $\mu$M BMS493 + 50 $\mu$M ATRA in 100 mM Gomori phosphate buffer, pH 8.0, containing 10% v/v EtOH that were incubated at 25 °C shaking at 300 rpm on a Thermomixer R (Eppendorf) for 2 h in the dark were spotted on Formvar/carbon-coated 400 mesh copper grids. Excesses volumes were removed by blotting with filter papers after 1 min at room temperature. Subsequently, the grids were rinsed with 5 $\mu$L of deionized water twice and 5 $\mu$L 1% w/v uranyl acetate; all the steps were blotted with filter papers immediately. The grids were finally negatively stained with 5 $\mu$L of 1% w/v uranyl acetate for 1 min before blotted with filter papers. Samples were viewed on a JEM-1400


DOI: 10.1021/acs.biomac.8b00158
*Biomacromolecules* 2018, 19, 1614−1624

transmission electron microscope (Jeol) and analyzed with ImageJ (NIH).[68]

**Chondrocyte Cultures.** Human articular chondrocytes were isolated from articular cartilage samples obtained from patients (donor age ranging from 48 to 67) undergoing total knee replacement surgery at NYU Langone Orthopedic Hospital. Knee cartilage was harvested from regions with no macroscopically evident degeneration. The collection of tissue from patients undergoing knee replacement surgery was approved by the Institutional Regulatory Board at NYU School of Medicine. Human chondrocytes were isolated from these cartilage samples as described by us.[69] Cells were plated at density of 1 × $10^6$ cells/well into 6-well tissue culture plate and cultured in DMEM containing 10% FCS, 2 mM L-glutamine, and 50 U/mL of penicillin and streptomycin (complete medium). After cells reached confluency, they were serum starved. 24 h after serum starvation, cells were treated with 200 nM ATRA, 10 ng/mL IL-1$\beta$, or ATRA together with IL-1$\beta$ for 72 h. In addition, cells were cultured in the absence or presence of 1 $\mu$M BMS493 or $C_{cc}^{S}$·BMS493.

**Quantitative Reverse Transcription Polymerase Chain Reaction (PCR) and Real-Time PCR Analyses.** Total RNA was isolated from chondrocyte cultures using the RNeasy minikit. mRNA levels of MMP-13 were quantified by real-time PCR as described previously.[70] Briefly, 1 $\mu$g of total RNA was reverse transcribed in a total volume of 30 $\mu$L by using an Omniscript RT kit. A 1:100 dilution of the cDNA resulting from the reverse transcription of 1 $\mu$g of total RNA was used as the template to quantify the relative content of mRNA by real-time PCR (StepOnePlus System, Applied Biosystems) with the appropriate primers and SYBR Green. PCRs were performed with a SYBR Green PCR Master Mix kit, with 95 °C for 10 min followed by 40 cycles at 95 °C for 15 s and 60 °C for 1 min, and 1 cycle at 95 °C for 15 s and 60 °C for 1 min. The 18S RNA was amplified at the same time and used as an internal control. The cycle threshold values for 18S RNA and the samples were measured and calculated by computer software. Relative transcript levels were calculated as $x = 2^{-\Delta\Delta Ct}$, in which $\Delta\Delta Ct = \Delta E - \Delta C$, $\Delta E = Ct_{exp} - Ct_{18S}$, and $\Delta C = Ct_{ctl} - Ct_{18S}$.

**Theoretical Hydrophobicity.** Hydrophobicities of BMS493, ATRA, and CCM were estimated with cLogP, logarithm of partition coefficient calculated on MarvinSketch (ChemAxon). The prediction applied a consensus method derived from both atom and fragment based models[71,72] and the PHYSPROP© database. The electrolyte concentration was neglected, and major tautomerization/resonance was considered.

**Statistical Analysis.** A student's *t*-test was applied to compare BMS493 alone and formulated in $C_{cc}^{S}$ by computing the mean MMP-13 expression levels and associated standard deviations of triplicates. A *p* value less than 0.05 is considered significant in independent statistical analysis.[73]

## RESULTS AND DISCUSSION

**Rationale.** Previously, we have demonstrated that $C_{cc}^{S}$ is capable of self-assembling into robust nanofibers and encapsulating the small molecule CCM.[40] While the pan-RAR inverse agonist, BMS493, bears promise for treatment of OA, it is hydrophobic and readily degradable. Since the hydrophobic pore is maintained and able to bind a range of small molecules,[41,59,60] we hypothesized that $C_{cc}^{S}$ could be employed to encapsulate and deliver BMS493. Moreover, $C_{cc}$ has been demonstrated to bind vitamin A, a reduced derivative of ATRA,[59] suggesting that $C_{cc}^{S?}$ could bind and sequester ATRA to reduce the induction of OA.

**Secondary Structural Analysis.** To assess the secondary structure of $C_{cc}^{S}$ in the presence of BMS493, ATRA, CCM, and mixtures thereof, wavelength scans were conducted via circular dichroism (CD). 50 $\mu$M BMS493 was applied to remain consistent with the equilibrated concentration in the binding studies, and equal molarity of ATRA was employed to allow for competition of binding to $C_{cc}^{S}$. In addition, to ensure the presence of 15 $\mu$M CCM introduced in the competitive binding assays did not disturb structural integrity, this condition was also investigated across the samples. As expected, $C_{cc}^{S}$ alone revealed a double minima with a $\theta_{208\,nm}$ and $\theta_{222\,nm}$ of −24 142.8 ± 334.2 deg·cm$^2$·dmol$^{-1}$ and −25 480.1 ± 183.5 deg·cm$^2$·dmol$^{-1}$, respectively, with a calculated helical content of 66.42 ± 0.48% (Figure 1a and Table 1). While the results

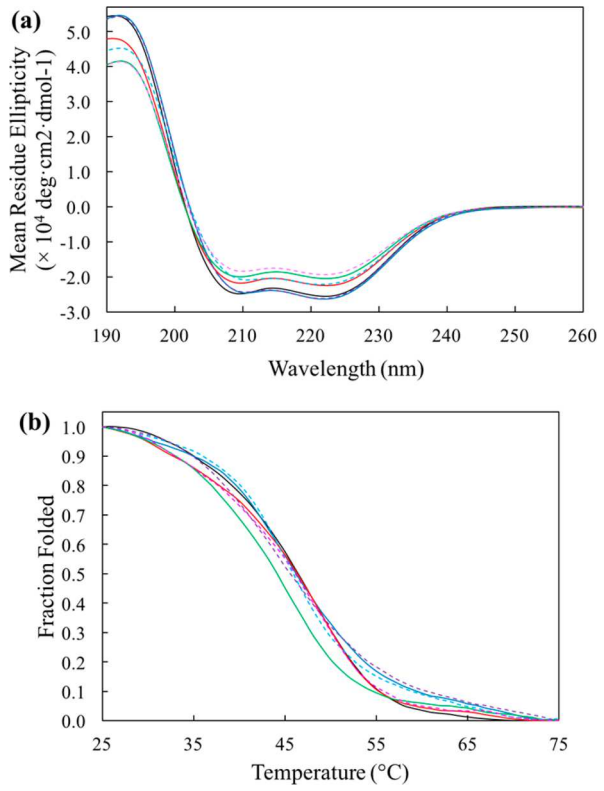


**Figure 1.** (a) Wavelength scans from 260 to 190 nm at 25 °C and (b) temperature scans at 222 nm from 25 to 75 °C of 10 $\mu$M $C_{cc}^{S}$ after incubating at 25 °C for 2 h shaking at 300 rpm in the dark with 50 $\mu$M BMS493 (blue solid), 50 $\mu$M ATRA (red solid), 15 $\mu$M CCM (green solid), 50 $\mu$M BMS493 + 15 $\mu$M CCM (cyan dashed), 50 $\mu$M ATRA + 15 $\mu$M CCM (magenta dashed), and 50 $\mu$M BMS493 + 50 $\mu$M ATRA (purple dashed) in 100 mM Gomori phosphate buffer, pH 8.0, containing 10% v/v EtOH (black solid). Data represent averages of three independent trials, where each study is average of three scans.

indicated a slightly improved conformation than previous published studies,[40,41] this increase could be attributed to the presence of the cosolvent 10% v/v EtOH[74,75] (Figure S2). In the presence of CCM, $C_{cc}^{S}$ exhibited a 13.0% loss in helicity with an overall $\theta_{208\,nm}$ and $\theta_{222\,nm}$ of −19 469.8 ± 588.5 deg·cm$^2$·dmol$^{-1}$ and −20 487.9 ± 559.8 deg·cm$^2$·dmol$^{-1}$, respectively (Figure 1a and Table 1). Similarly, the addition of ATRA to $C_{cc}^{S}$ led to a reduction in helicity by 8.0% with a $\theta_{208\,nm}$ of −21 068.8 ± 619.5 deg·cm$^2$·dmol$^{-1}$ and $\theta_{222\,nm}$ of −22 432.2 ± 796.7 deg·cm$^2$·dmol$^{-1}$ (Figure 1a and Table 1). By contrast, the presence of BMS493 improved the helical content of $C_{cc}^{S}$ by 2.1% with a $\theta_{208\,nm}$ and $\theta_{222\,nm}$ of −22 823.8 ± 182.2 deg·cm$^2$·dmol$^{-1}$ and −26 295.0 ± 233.3 deg·cm$^2$·dmol$^{-1}$, respectively (Figure 1a and Table 1), similar to the introduction of ATRA with BMS493. However, the incubation of $C_{cc}^{S}$ with CCM and ATRA led to a substantial loss in helical content by 15.7% with a $\theta_{208\,nm}$ of −17 644.5 ± 1101.9 deg·cm$^2$·dmol$^{-1}$ and $\theta_{222\,nm}$ of −19 447.3 ± 815.6 deg·cm$^2$·dmol$^{-1}$ (Figure 1a and Table 1).



DOI: 10.1021/acs.biomac.8b00158
Biomacromolecules 2018, 19, 1614−1624

Table 1. Summary of Structure, Thermal Stability, and Thermodynamic Parameters of $C_{cc}^{S}$ in the Absence and Presence of Small Molecules[a]

| 50 μM BMS493 | 50 μM ATRA | 15 μM CCM | $-\theta_{208\,nm}$ (deg·cm$^2$·dmol$^{-1}$) | $-\theta_{222\,nm}$ (deg·cm$^2$·dmol$^{-1}$) | helical content (%) | $T_m$ (°C) | $-\Delta H°$ (kcal·mol$^{-1}$) | $\Delta S°$ (kcal·mol$^{-1}$·K$^{-1}$) | $-\Delta G°$ (kcal·mol$^{-1}$) |
|---|---|---|---|---|---|---|---|---|---|
| − | − | − | 24,142.8 ± 334.2 | 25,480.1 ± 183.5 | 66.42 ± 0.48 | 47.00 ± 1.00 | 50.48 ± 2.28 | 0.16 ± 0.01 | 3.47 ± 0.26 |
| + | − | − | 22,823.8 ± 182.2 | 26,295.0 ± 233.3 | 68.55 ± 0.61 | 47.00 ± 1.00 | 38.36 ± 1.28 | 0.12 ± 0.00 | 2.64 ± 0.06 |
| − | + | − | 21,068.8 ± 19.5 | 22,432.2 ± 796.7 | 58.48 ± 2.08 | 46.67 ± 1.15 | 42.91 ± 1.48 | 0.13 ± 0.00 | 2.91 ± 0.24 |
| − | − | + | 19,469.8 ± 588.5 | 20,487.9 ± 559.8 | 53.41 ± 1.46 | 44.67 ± 0.58 | 38.46 ± 2.30 | 0.12 ± 0.01 | 2.38 ± 0.19 |
| + | − | + | 19,295.8 ± 647.7 | 22,103.7 ± 914.7 | 57.62 ± 2.38 | 46.67 ± 0.58 | 42.52 ± 1.54 | 0.13 ± 0.01 | 2.88 ± 0.06 |
| − | + | + | 17,644.5 ± 101.9 | 19,447.3 ± 815.6 | 50.70 ± 2.13 | 46.67 ± 0.58 | 42.34 ± 2.26 | 0.13 ± 0.01 | 2.87 ± 0.14 |
| + | + | − | 22,830.4 ± 208.8 | 26,122.8 ± 510.6 | 68.10 ± 1.33 | 46.33 ± 0.58 | 38.13 ± 3.58 | 0.12 ± 0.01 | 2.55 ± 0.31 |

[a]Data represent averages of three independent studies, where each study is an average of three scans of measurement.

Likewise, $C_{cc}^{S}$ in the presence of both CCM and BMS493 revealed a reduction in helicity by 8.8% with an overall $\theta_{208\,nm}$ and $\theta_{222\,nm}$ of −19 295.8 ± 647.7 deg·cm$^2$·dmol$^{-1}$ and −22 103.7 ± 914.7 deg·cm$^2$·dmol$^{-1}$, respectively (Figure 1a and Table 1). In general, the addition of CCM alone as well as combined with BMS493 or ATRA negatively affected $C_{cc}^{S}$ structure, whereas introduction of BMS493 alone and mixed with ATRA improved the helical content.

**Stability Analysis and Interplay with Structure.** The impact of small molecule on stability was assessed by monitoring the signal at 222 nm as a function of temperature (Figure 1b). In the absence of small molecule, $C_{cc}^{S}$ exhibited a melting temperature ($T_m$) of 47.00 ± 1.00 °C (Figure 1b and Table 1), confirming previous work.[40,41] In the presence of CCM, $C_{cc}^{S}$ revealed a slight decrease in $T_m$ by 2.33 °C, whereas the addition of BMS493, ATRA, and all mixtures maintained its thermal stability (Figure 1b and Table 1). Consistent with the literature,[41,42] $C_{cc}^{S}$ demonstrated a reversibility of folding after undergoing a melting process in the absence and presence of all small molecules (Figure S3 and Table S1), suggesting the two-state mechanism of unfolding was preserved along with the monophasic behavior of melting.[76−78] The thermodynamic parameters were calculated based on fraction folded ($F$) and $T_m$ (Table 1).[79] While $C_{cc}^{S}$ alone exhibited −50.48 ± 2.28 kcal·mol$^{-1}$ in van't Hoff enthalpy ($\Delta H°$) and Gibbs free energy ($\Delta G°$) of −3.47 ± 0.26 kcal·mol$^{-1}$, the small molecules caused instability by raising $\Delta G°$ of 0.5−1.0 kcal·mol$^{-1}$ (Table 1). Despite that $C_{cc}^{S}$ remained highly structured when bound to BMS493, the overall thermodynamic stability was reduced, with a $\Delta G°$ to −2.64 ± 0.06 kcal·mol$^{-1}$ (Table 1). By contrast, ATRA caused less disturbance to $C_{cc}^{S}$ with $\Delta G°$ of −2.91 ± 0.24 kcal·mol$^{-1}$ (Table 1). In the presence of both BMS493 and ATRA, $\Delta G°$ was further destabilized to −2.55 ± 0.31 kcal·mol$^{-1}$ (Table 1). Since CCM negatively impacted the structural and thermodynamic properties, the largest destabilization was observed, exhibiting a $\Delta G°$ of −2.38 ± 0.19 kcal·mol$^{-1}$ (Table 1). However, when coexisting with BMS493 or ATRA, the $\Delta G°$ relative to CCM alone improved to −2.88 ± 0.06 and −2.87 ± 0.14 kcal·mol$^{-1}$, respectively (Table 1).

Several coiled-coil systems such as human COMP[76,80] and the leucine zipper[81] have suggested a relationship between Gibbs free energy and oligomerization level. The structural studies for CCM mixed with BMS493 or ATRA have been performed to assess the conformation and stability of $C_{cc}^{S}$ for the competition binding studies. The presence of CCM alone causes a decrease in $\alpha$-helical content of $C_{cc}^{S}$, while also contributing to greatest destabilization in overall $\Delta G°$ (Figure 1a and Table 1) of ∼1.0 kcal·mol$^{-1}$. Addition of BMS493 or ATRA to the bound $C_{cc}^{S}$·CCM complex improves the $\Delta G°$ (Figure 1a and Table 1), indicating that these two small molecules would better interact with the protein.

$C_{cc}^{S}$ exhibits a decrease in $\Delta G°$ when bound to BMS493 relative to unbound free $C_{cc}^{S}$ (Table 1), indicating the accommodation of BMS493 in the hydrophobic region disturbs the association among monohelices. However, the helicity is improved in the presence of BMS493 (Figure 1a and Table 1). Ethanol can alter conformational flexibility to initiate the helix formation because alcohols do not adequately satisfy the H-bond potential at the amide groups of the peptide.[74] For $\alpha$-helices in particular, studies have revealed that alcohol molecules are typically bound toward the N-terminus,[74,75] where the net charge is positive due to dipole moment of the helix,[82] promoting interactions with electronegative groups


DOI: 10.1021/acs.biomac.8b00158
Biomacromolecules 2018, 19, 1614−1624

such as the alcohol moiety. The 10% ethanol content in the formulation may provide flexibility to accommodate BMS493. By contrast, the presence of ATRA leads to a loss in helical content while minimally impacting the $\Delta G°$ (Figure 1a and Table 1). While the ATRA destabilizes the helical structure, oligomeric association is marginally affected. The coexistence of BMS493 and ATRA preserves the helical content of $C_{cc}^{S}$ while significantly decreasing $\Delta G°$ (Figure 1a and Table 1). The competition and exchange of both small molecules may be contributing to the overall destabilization of the association of monohelices. Overall, the results indicate that the secondary structure of $C_{cc}^{S}$ is not significantly compromised, despite the small molecules destabilizing the oligomeric states as demonstrated by increased Gibbs free energy. Moreover, the helicity is well maintained in the presence of BMS493 and moderately decreases when bound to ATRA.

**Binding Studies.** In order to assess the binding ability of $C_{cc}^{S}$ to each small molecule, the dissociation constants ($K_d$) were measured for BMS493, ATRA, and CCM. Consistent with our previous studies on specific hydrophobic residues including L37, L44, V47, and L51 for *all-trans*-retinol (ATR, vitamin A) binding,[41] Guo et al. demonstrated that ATR is accommodated within the N-terminal region of $C_{cc}$ via X-ray crystallography while also determining binding to ATRA via a competition assay with ATR.[59] These residues have been identified as essential to binding CCM, promoting CCM to be used as an appropriate probe in the competition binding assays. The $K_d$ of $C_{cc}^{S}$ for CCM was primarily determined to be 16.82 ± 0.13 $\mu$M (Figure S4a and Table 2). Through competition experiment,

**Table 2. Summary of Binding Affinity of the Small Molecules to 10 $\mu$M $C_{cc}^{S}$ Presented with $K_d$ ($\mu$M)[a]**

| | BMS493 | ATRA | CCM |
|---|---|---|---|
| study 1 | 13.437 ± 0.051 | 3.641 ± 0.096 | 16.770 ± 0.665 |
| study 2 | 12.367 ± 0.010 | 3.320 ± 0.092 | 16.957 ± 0.165 |
| study 3 | 12.030 ± 0.036 | 3.316 ± 0.092 | 16.720 ± 0.250 |
| average | 12.278 ± 0.218 | 3.426 ± 0.186 | 16.816 ± 0.125 |

[a]Data represent three independent studies for each small molecule, where each study is an average of triplicates.

the fluorescence of CCM decreased along with increasing concentration of BMS493 (Figure 2a and Figure S4b) or ATRA (Figure 2b and Figure S4c), and the $K_d$ values were computed at 12.28 ± 0.22 and 3.43 ± 0.19 $\mu$M for BMS493 and ATRA, respectively (Figure S4 and Table 2). Thus, relative to CCM, $C_{cc}^{S}$ exhibited approximately 5-fold higher affinity to ATRA and a 1.4-fold improved binding to BMS493.

The structural studies by Guo et al. suggested BMS493 might bind $C_{cc}^{S}$ at different sites from ATRA[59] and possibly toward the C-terminus.[41] This assumption was verified with a competition binding assay for BMS493 with CCM; the affinity for BMS493 was moderately higher than CCM with 1.4-fold lower $K_d$ (Figure 2a,b). In addition, the estimated theoretical logarithm of partition coefficient, cLogP, for the BMS493, ATRA, and CCM was computed as 7.64, 4.47, and 3.76, respectively. By profiling the average surrounding hydrophobicity of individual residues of $C_{cc}^{S}$ on ProtScale (ExPASy),[83] approximately 10 positions located near the C-terminus scored higher relative to the N-terminal region. These computations along with the structural studies suggest that BMS493 would be accommodated in the C-terminal cavity attributing to nonspecific hydrophobic interaction. By contrast,

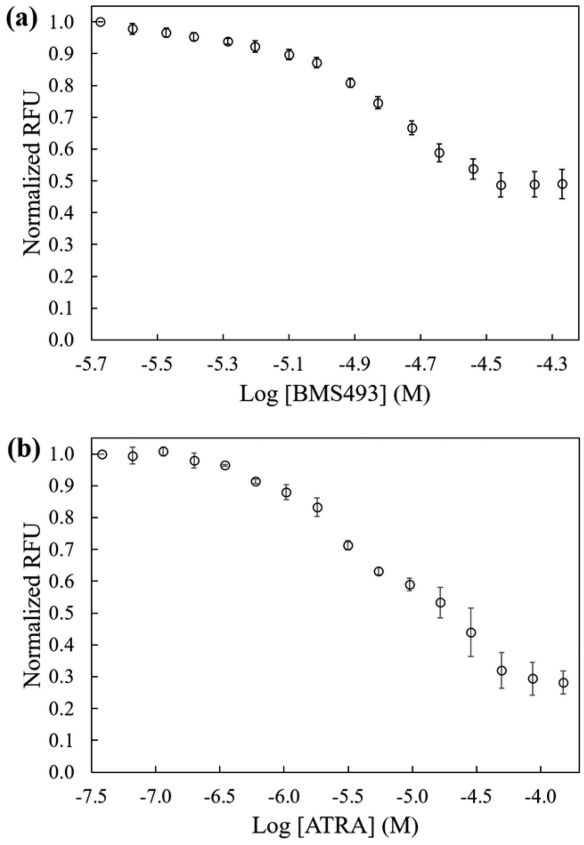


**Figure 2.** Competitive binding curves of 10 $\mu$M $C_{cc}^{S}$ in the presence of (a) 1.98 to 50 $\mu$M BMS493 and (b) 0.04 to 150 $\mu$M ATRA outcompeting 15 $\mu$M CCM in 100 mM Gomori phosphate buffer, pH 8.0, containing 10% v/v EtOH. Relative fluorescence units (RFU) were measured for emission at 490 nm upon excited at 420 nm and normalized. Data represent averages of three independent assays, where each assay is an average of triplicates.

CCM with about half the cLogP value of BMS493 would rely on more specific interactions with the residues such as V65 and S68 identified in our previous study,[41] leading to the observed lower affinity for $C_{cc}^{S}$ than BMS493. Moreover, while competing with approximately 70% saturation of CCM, ATRA demonstrated an ~30% fluorescence at equilibrium (Figure 2b and Figure S4c); this residual fluorescence could be due to CCM bound to $C_{cc}^{S}$ at the C-terminus. Correspondingly, $C_{cc}^{S}$ bound CCM at the N-terminus as well, as ~50% fluorescent intensity was observed at the equilibrium of BMS493 binding (Figure 2a and Figure S4b).

We further correlated $K_d$ values of the small molecules with the Gibbs free energies, and a highly linear relationship with a $R^2$ of 0.98 (Figure S6) was obtained, demonstrating that stabilization in fact favors higher affinity. The poorest binder, CCM, exhibited the greatest perturbation to the assembly of the monohelices. This was followed by BMS493 bearing both intermediate affinity for $C_{cc}^{S}$ and thermodynamic stabilization. The best binder, ATRA, demonstrated the preservation of self-assembly.

**Morphological Studies.** Consistent with previous studies, $C_{cc}^{S}$ self-assembled into nanofibers of 13.48 ± 2.82 nm in diameter (Figure 3a and Table 3). When 10% v/v EtOH was introduced, $C_{cc}^{S}$ nanofibers increased the diameters by ~5-fold to 69.86 ± 16.86 nm (Figure 3b and Table 3). In the presence of BMS493 or ATRA, $C_{cc}^{S}$ exhibited diameters of 11.11 ± 2.79


DOI: 10.1021/acs.biomac.8b00158
Biomacromolecules 2018, 19, 1614−1624

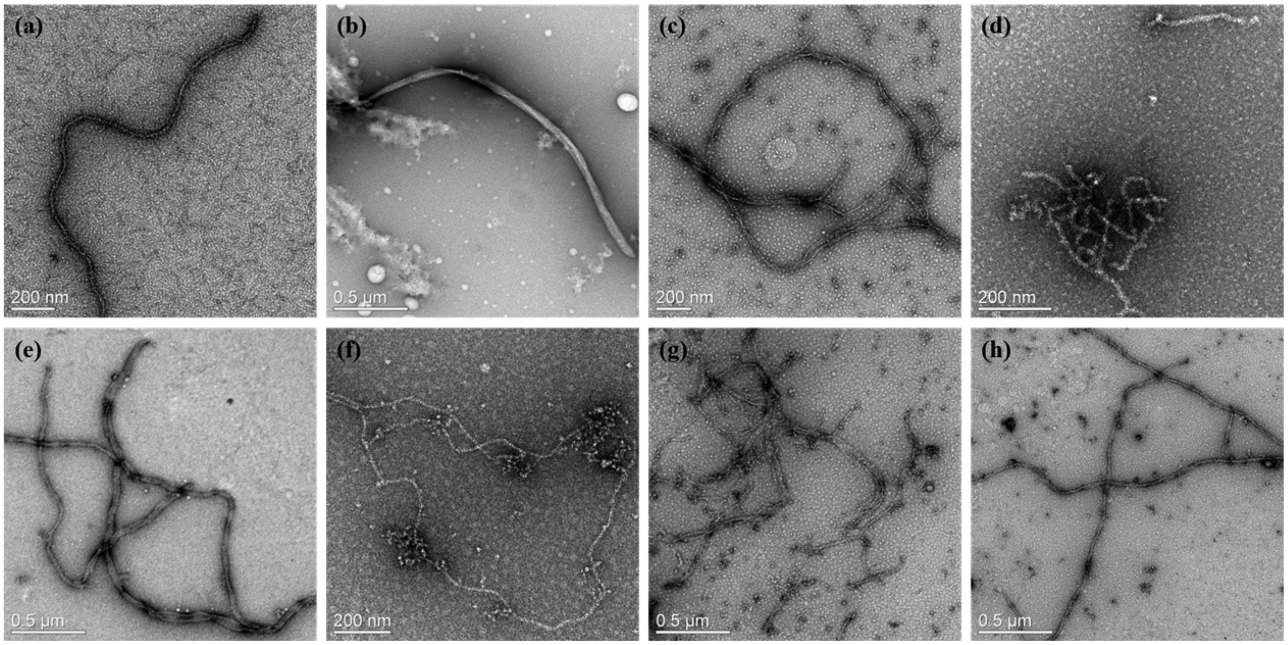


**Figure 3.** TEM images of 10 $\mu$M $C_{cc}^{S}$ in (a) 100 mM Gomori phosphate buffer, pH 8.0, and in the presence of (b) 10% v/v EtOH, (c) 50 $\mu$M BMS493, (d) 50 $\mu$M ATRA, (e) 15 $\mu$M CCM, (f) 50 $\mu$M BMS493 + 50 $\mu$M ATRA, (g) 50 $\mu$M BMS493 + 15 $\mu$M CCM, and (h) 50 $\mu$M ATRA + 15 $\mu$M CCM.

**Table 3. Summary of Diameters of $C_{cc}^{S}$ in the Absence and Presence of Small Molecules**

| | | | | | | | | |
|---|---|---|---|---|---|---|---|---|
| 10% v/v EtOH | – | + | | | | | | |
| 50 $\mu$M BMS | – | – | + | – | – | + | – | + |
| 50 $\mu$M ATRA | – | – | – | + | – | – | + | + |
| 15 $\mu$M CCM | – | – | – | – | + | + | + | – |
| diameter (nm) | 13.48 ± 2.82 | 69.86 ± 16.86 | 11.11 ± 2.79 | 15.07 ± 1.84 | 42.35 ± 9.86 | 9.95 ± 1.35 | 24.21 ± 3.47 | 11.97 ± 9.86 |
| $N^a$ | 56 | 22 | 127 | 66 | 79 | 143 | 83 | 72 |

[a] $N$ represents the number of fibers measured to obtain the average diameter values.

nm (Figure 3c and Table 3) and 15.07 ± 1.84 nm (Figure 3d and Table 3), respectively, similar to the nanofibers in the aqueous buffer without EtOH content. $C_{cc}^{S}$ in the presence of CCM formed nanofibers with larger diameters of 42.35 ± 9.86 nm (Figure 3e and Table 3); however, the sizes reduced to 9.95 ± 1.35 and 24.21 ± 3.47 nm when CCM was mixed with BMS493 and ATRA, respectively (Figure 3g,h and Table 3). Incubated with BMS493 and ATRA together, the $C_{cc}^{S}$ nanofibers maintained their size with diameters of 11.97 ± 2.39 nm (Figure 3f and Table 3). Overall, the presence of BMS493 and ATRA retained $C_{cc}^{S}$ nanofiber size, whereas EtOH or CCM alone increased the nanofiber diameter by 3−5-fold.

We have previously demonstrated that $C_{cc}^{S}$ in 10 mM phosphate buffer, pH 8.0, self-assembled into fibers of 10−15 nm in diameter.[40] On the basis of our structural studies, we expected $C_{cc}^{S}$ would preserve nanofiber formation and under all conditions; this was the case (Figure 3). Notably, in the presence of 10% ethanol and CCM, thicker fibers were observed. Since ethanol molecules enhance the helical structure of $C_{cc}^{S}$ via H-bonds in the interior, the stabilization of the assemblies could allow the nanofibers to further bundle into larger diameters by >5-fold (Figure 3b). Similarly, CCM caused the H-bond effect, facilitating further assembly to generate nanofibers with 3-fold greater diameters (Figure 3e). Through the TEM imaging, we confirmed that $C_{cc}^{S}$ can maintain the nanofiber formation in the presence of various small molecules; despite the difference in diameter, the oligomerization of $C_{cc}^{S}$ as well as the nanoscale assembly of fibers were not compromised.

***In Vitro* Chondrocyte Treatment.** To assess the efficacy of $C_{cc}^{S}$·BMS493 complex and compare it to the treatment of BMS493 alone, MMP-13 mRNA levels were quantified. MMP-13 is one of the major metalloproteinases expressed in OA cartilage that contributes to cartilage degradation.[84] In addition, 200 nM ATRA and 10 ng/mL IL-1$\beta$ were employed as catabolic stimulators, which significantly promoted MMP-13 expression.[85] As a control, endotoxin-free $C_{cc}^{S}$ alone was introduced to chondrocytes, revealing virtually similar outcomes to the buffer control in the absence and presence of ATRA and/or IL-1$\beta$. The $C_{cc}^{S}$·BMS493 exhibited decreased MMP-13 mRNA level in the IL-1$\beta$ stimulated chondrocytes by 21.5%, while more effective downregulation was observed in the ATRA as well as ATRA + IL-1$\beta$ stimulated chondrocytes by 63.0% and 64.1%, respectively (Figure 4). Compared to the $C_{cc}^{S}$·BMS493, BMS493 alone revealed a 52.6% decrease in MMP-13 mRNA level only in the presence of ATRA + IL-1$\beta$, whereas no significant effect was observed for ATRA or IL-1$\beta$ alone (Figure 4). These findings demonstrate that the $C_{cc}^{S}$·BMS493 improved the downregulation of MMP-13 mRNA.

Normal chondrocytes remain as resting cells to form articular cartilage. During OA pathogenesis, articular chondrocytes increase the expression of MMP-13, the main protease responsible for the degradation of type II collagen.[84] ATRA has been previously shown to stimulate MMP-13 expression in


DOI: 10.1021/acs.biomac.8b00158
Biomacromolecules 2018, 19, 1614−1624

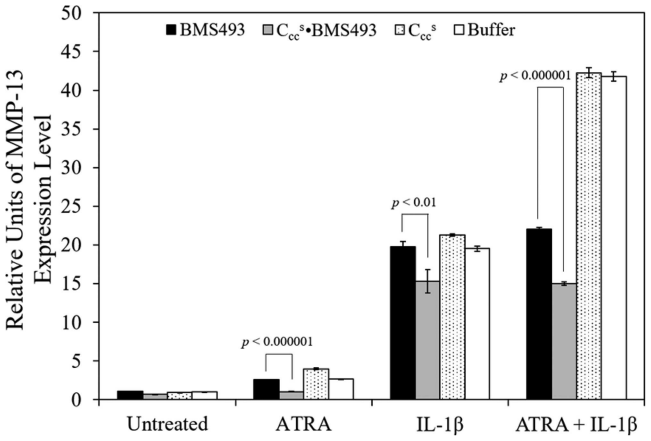


**Figure 4.** Efficacy of BMS493 alone (solid black) and bound to $C_{cc}^{S}$ (gray) for the downregulation of MMP-13 expression of chondrocytes stimulated by 200 nM ATRA and/or 10 ng/mL IL-1$\beta$, in comparison of 100 nM $C_{cc}^{S}$ alone (dots) after 3 days. All the treatments were prepared in 100 mM Gomori phosphate buffer, pH 8.0, in the presence of 10% (v/v) EtOH (solid white) prior to 100-fold dilution into chondrocyte media. Levels of mRNA were determined by real-time PCR using SYBR Green and normalized to the level of 18S RNA. The mRNA levels are expressed relative to the level of vehicle-treated cells (untreated), which was set as 1. Data were obtained from triplicate PCRs using RNA from three different cultures ($n$ = 3). Values represent mean ± standard deviation.

chondrocytes.[86,87] In this study we show that ATRA increased the mRNA levels of MMP-13 in human articular chondrocytes, confirming a previous study showing increased MMP-13 levels in human cartilage explants treated with ATRA. In addition, our results demonstrate that ATRA together with IL-1$\beta$, a major proinflammatory cytokine in OA,[88] showed the highest mRNA levels of MMP-13 in human articular chondrocytes. BMS493 alone was not effective to downregulate MMP-13 of ATRA stimulated chondrocytes, whereas $C_{cc}^{S}$ BMS493 improved downregulation by ~3-fold, indicating that $C_{cc}^{S}$ prevents BMS493 degradation. $C_{cc}^{S}$·BMS493 was also more efficient in decreasing the mRNA levels of MMP-13 in chondrocytes, which were treated with IL-1$\beta$ or ATRA together with IL-1$\beta$ than BMS493 alone. The increase in helical content in the presence of BMS493 suggests a binding and direct interaction of the therapeutic with $C_{cc}^{S}$, which protects BMS493 under physiological conditions. In addition to supporting that BMS493 was protected by $C_{cc}^{S}$, it was released in a sustained manner from $C_{cc}^{S}$ during the three-day treatment.

## CONCLUSIONS

Herein, we have demonstrated that $C_{cc}^{S}$ protects and delivers BMS493 *in vitro* for treatment of articular chondrocytes, which were exposed to ATRA, IL-1$\beta$, or ATRA together with IL-1$\beta$. $C_{cc}^{S}$ is able to encapsulate and deliver without compromising its stability, structure, and morphology in the presence of BMS493. As ATRA exhibits higher affinity toward $C_{cc}^{S}$ than BMS493, the high content of ATRA in an OA joint could serve as a driving force to release BMS493, adjusting the dosage during the treatment depending on severity. Some mechanisms of drug release upon administration have been simulated, and competitive displacement of endogenous materials has been suggested critical for the cases where simple dilution is minimal[89] due to low solubility of the drug for instance. To the best of our knowledge, this is the first study to assess BMS493 as a potential therapeutics for the treatment of OA. This work provides a framework to enhance the delivery of additional compounds relevant to OA-associated RAR pathways. Future work to optimize biophysical properties of $C_{cc}^{S}$ to better enable the delivery of BMS493 and other RAR-related compounds, increasing its stability or loading capacity, is underway.

## ASSOCIATED CONTENT

### Supporting Information

The Supporting Information is available free of charge on the ACS Publications website at DOI: 10.1021/acs.biomac.8b00158.

SDS-PAGE of $C_{cc}^{S}$ purification; CD spectra and temperature scans of $C_{cc}^{S}$ in the absence of EtOH, and reversed CD measurements of $C_{cc}^{S}$ in the presence of EtOH and the small molecules; plots of binding studies; sizing of TEM images; correlation between affinity and Gibbs free energy (PDF)

## AUTHOR INFORMATION


### Corresponding Authors

*E-mail: montclare@nyu.edu (J.K.M.).
*E-mail: thorsten.kirsch@nyumc.org (T.K.).

### ORCID

Jin K. Montclare: 0000-0001-6857-3591

### Present Addresses

A.S.A.: Chemical Biology Program, Memorial Sloan Kettering Cancer Center, New York, NY 10065.
C.Y.: Department of Life Sciences and Healthcare, NYC Economic Development Corporation, New York, NY 10038.
T.M.: Department of Physiology and Regenerative Medicine, Kindai University School of Medicine, Osaka, Japan.


### Notes

The authors declare no competing financial interest.

## ACKNOWLEDGMENTS

This work was supported by a Pilot Project grant from the Clinical and Translational Science Institute at NYU School of Medicine (NIH/NCATS UL1 TR000038) and in part by NSF (DMR-1728858) and the NSF MRSEC Program under Award DMR-1420073. A.S.A. was supported by the Indonesia Endowment Fund for Education. Electron microscopic analysis used resources of the Center for Functional Nanomaterials, which is a U.S. DOE Office of Science Facility at Brookhaven National Laboratory under Contract DE-SC0012704.

## REFERENCES


(1) Anderson, A. S.; Loeser, R. F. Why is osteoarthritis an age-related disease? *Best Pract. Res. Clin. Rheumatol.* **2010**, *24* (1), 15−26.
(2) Lotz, M. K. New developments in osteoarthritis: posttraumatic osteoarthritis: pathogenesis and pharmacological treatment options. *Arthrit. Res. Ther.* **2010**, *12* (3), 211.
(3) Issa, R. I.; Griffin, T. M. Pathobiology of obesity and osteoarthritis: integrating biomechanics and inflammation. *Pathobiol. Aging Age-Relat. Dis.* **2012**, *2*, 17470.
(4) Nelson, F.; Dahlberg, L.; Laverty, S.; Reiner, A.; Pidoux, I.; Ionescu, M.; Fraser, G. L.; Brooks, E.; Tanzer, M.; Rosenberg, L. C.; Dieppe, P.; Robin Poole, A. Evidence for altered synthesis of type II collagen in patients with osteoarthritis. *J. Clin. Invest.* **1998**, *102* (12), 2115.




DOI: 10.1021/acs.biomac.8b00158
*Biomacromolecules* 2018, 19, 1614−1624

(5) Inerot, S.; Heinegård, D.; Audell, L.; Olsson, S. Articular-cartilage proteoglycans in aging and osteoarthritis. *Biochem. J.* **1978**, *169* (1), 143−156.
(6) Troeberg, L.; Nagase, H. Proteases involved in cartilage matrix degradation in osteoarthritis. *Biochim. Biophys. Acta, Proteins Proteomics* **2012**, *1824* (1), 133−145.
(7) Goldring, M. B. The role of the chondrocyte in osteoarthritis. *Arthritis Rheum.* **2000**, *43* (9), 1916−1926.
(8) Van der Kraan, P.; Van den Berg, W. Chondrocyte hypertrophy and osteoarthritis: role in initiation and progression of cartilage degeneration? *Osteoarthritis Cartilage* **2012**, *20* (3), 223−232.
(9) Kirsch, T.; Swoboda, B.; Nah, H.-D. Activation of annexin II and V expression, terminal differentiation, mineralization and apoptosis in human osteoarthritic cartilage. *Osteoarthritis Cartilage* **2000**, *8* (4), 294−302.
(10) Tchetina, E. V.; Kobayashi, M.; Yasuda, T.; Meijers, T.; Pidoux, I.; Poole, A. R. Chondrocyte hypertrophy can be induced by a cryptic sequence of type II collagen and is accompanied by the induction of MMP-13 and collagenase activity: implications for development and arthritis. *Matrix Biol.* **2007**, *26* (4), 247−258.
(11) Merz, D.; Liu, R.; Johnson, K.; Terkeltaub, R. IL-8/CXCL8 and growth-related oncogene $\alpha$/CXCL1 induce chondrocyte hypertrophic differentiation. *J. Immunol.* **2003**, *171* (8), 4406−4415.
(12) Pfander, D.; Swoboda, B.; Kirsch, T. Expression of early and late differentiation markers (proliferating cell nuclear antigen, syndecan-3, annexin VI, and alkaline phosphatase) by human osteoarthritic chondrocytes. *Am. J. Pathol.* **2001**, *159* (5), 1777−1783.
(13) Davies, M. R.; Ribeiro, L. R.; Downey-Jones, M.; Needham, M. R.; Oakley, C.; Wardale, J. Ligands for retinoic acid receptors are elevated in osteoarthritis and may contribute to pathologic processes in the osteoarthritic joint. *Arthritis Rheum.* **2009**, *60* (6), 1722−1732.
(14) Dreier, R. Hypertrophic differentiation of chondrocytes in osteoarthritis: the developmental aspect of degenerative joint disorders. *Arthrit. Res. Ther.* **2010**, *12* (5), 216.
(15) Mangelsdorf, D. J.; Ong, E. S.; Dyck, J. A.; Evans, R. M. Nuclear receptor that identifies a novel retinoic acid response pathway. *Nature* **1990**, *345* (6272), 224−229.
(16) Chambon, P. A decade of molecular biology of retinoic acid receptors. *FASEB J.* **1996**, *10* (9), 940−954.
(17) Koyama, E.; Golden, E. B.; Kirsch, T.; Adams, S. L.; Chandraratna, R. A.; Michaille, J.-J.; Pacifici, M. Retinoid signaling is required for chondrocyte maturation and endochondral bone formation during limb skeletogenesis. *Dev. Biol.* **1999**, *208* (2), 375−391.
(18) Germain, P.; Iyer, J.; Zechel, C.; Gronemeyer, H. Co-regulator recruitment and the mechanism of retinoic acid receptor synergy. *Nature* **2002**, *415* (6868), 187−192.
(19) De Lera, A. R.; Bourguet, W.; Altucci, L.; Gronemeyer, H. Design of selective nuclear receptor modulators: RAR and RXR as a case study. *Nat. Rev. Drug Discovery* **2007**, *6* (10), 811−820.
(20) Germain, P.; Gaudon, C.; Pogenberg, V.; Sanglier, S.; Van Dorsselaer, A.; Royer, C. A.; Lazar, M. A.; Bourguet, W.; Gronemeyer, H. Differential action on coregulator interaction defines inverse retinoid agonists and neutral antagonists. *Chem. Biol.* **2009**, *16* (5), 479−489.
(21) Bourguet, W.; de Lera, A. R.; Gronemeyer, H. Inverse agonists and antagonists of retinoid receptors. *Methods Enzymol.* **2010**, *485*, 161−195.
(22) Allen, T. M.; Cullis, P. R. Liposomal drug delivery systems: from concept to clinical applications. *Adv. Drug Delivery Rev.* **2013**, *65* (1), 36−48.
(23) Ahmad, Z.; Shah, A.; Siddiq, M.; Kraatz, H.-B. Polymeric micelles as drug delivery vehicles. *RSC Adv.* **2014**, *4* (33), 17028−17038.
(24) Schmaljohann, D. Thermo-and pH-responsive polymers in drug delivery. *Adv. Drug Delivery Rev.* **2006**, *58* (15), 1655−1670.
(25) Kim, S.; Kim, J.-H.; Jeon, O.; Kwon, I. C.; Park, K. Engineered polymers for advanced drug delivery. *Eur. J. Pharm. Biopharm.* **2009**, *71* (3), 420−430.
(26) Liggins, R.; Cruz, T.; Min, W.; Liang, L.; Hunter, W.; Burt, H. Intra-articular treatment of arthritis with microsphere formulations of paclitaxel: biocompatibility and efficacy determinations in rabbits. *Inflammation Res.* **2004**, *53* (8), 363−372.
(27) Ratcliffe, J.; Hunneyball, I.; Smith, A.; Wilson, C.; Davis, S. Preparation and evaluation of biodegradable polymeric systems for the intra-articular delivery of drugs. *J. Pharm. Pharmacol.* **1984**, *36* (7), 431−436.
(28) Nishide, M.; Kamei, S.; Takakura, Y.; Tamai, S.; Tabata, Y.; Ikada, Y. Fate of biodegradable DL-lactic acid oligomer microspheres in the articulus. *J. Bioact. Compat. Polym.* **1999**, *14* (5), 385−398.
(29) Katdare, A.; Chaubal, M. *Excipient Development for Pharmaceutical, Biotechnology, and Drug Delivery Systems*; CRC Press: 2006.
(30) Butoescu, N.; Jordan, O.; Doelker, E. Intra-articular drug delivery systems for the treatment of rheumatic diseases: a review of the factors influencing their performance. *Eur. J. Pharm. Biopharm.* **2009**, *73*, 205−218.
(31) Yin, L.; Yuvienco, C.; Montclare, J. K. Protein Based Drug Delivery Agents: Contemporary Developments and Challenges. *Biomaterials* **2017**, *134*, 91−116.
(32) Wu, Y.; Collier, J. H. $\alpha$-Helical coiled-coil peptide materials for biomedical applications. *Wiley Interdiscip. Rev.: Nanomed. Nanobiotechnol.* **2017**, *9* (2), e1424.
(33) Frezzo, J. A.; Montclare, J. K. Exploring the potential of engineered coiled-coil protein microfibers in drug delivery. *Ther. Delivery* **2015**, *6* (6), 643−646.
(34) Woolfson, D. N. Coiled-Coil Design: Updated and Upgraded. In *Fibrous Proteins: Structures and Mechanisms*; Springer: 2017; pp 35−61.
(35) Eriksson, M.; Hassan, S.; Larsson, R.; Linder, S.; Ramqvist, T.; Lövborg, H.; Vikinge, T.; Figgemeier, E.; Müller, J.; Stetefeld, J. Utilization of a Right-handed Coiled-coil Protein from Archaebacterium Staphylothermus marinus as a Carrier for Cisplatin. *Anticancer Res.* **2009**, *29* (1), 11−18.
(36) Fan, X.; Zhao, F.; Wang, X.; Wu, G. Doxorubicin-triggered self-assembly of native amphiphilic peptides into spherical nanoparticles. *Oncotarget* **2016**, *7* (36), 58445.
(37) Ding, L.; Jiang, Y.; Zhang, J.; Klok, H.-A.; Zhong, Z. pH-Sensitive Coiled-Coil Peptide-Cross-Linked Hyaluronic Acid Nanogels: Synthesis and Targeted Intracellular Protein Delivery to CD44 Positive Cancer Cells. *Biomacromolecules* **2018**, *19* (2), 555−562.
(38) Pechar, M.; Pola, R.; Janoušková, O.; Sieglová, I.; Král, V.; Fábry, M.; Tomalová, B.; Kovář, M. Polymer cancerostatics targeted with an antibody fragment bound via a coiled coil motif: In vivo therapeutic efficacy against murine BCL1 leukemia. *Macromol. Biosci.* **2018**, *18* (1), 1700173.
(39) Wu, K.; Yang, J.; Liu, J.; Kopeček, J. Coiled-coil based drug-free macromolecular therapeutics: in vivo efficacy. *J. Controlled Release* **2012**, *157* (1), 126−131.
(40) Gunasekar, S. K.; Anjia, L.; Matsui, H.; Montclare, J. K. Effects of Divalent Metals on Nanoscopic Fiber Formation and Small Molecule Recognition of Helical Proteins. *Adv. Funct. Mater.* **2012**, *22* (10), 2154−2159.
(41) Gunasekar, S. K.; Asnani, M.; Limbad, C.; Haghpanah, J. S.; Hom, W.; Barra, H.; Nanda, S.; Lu, M.; Montclare, J. K. N-Terminal Aliphatic Residues Dictate the Structure, Stability, Assembly, and Small Molecule Binding of the Coiled-Coil Region of Cartilage Oligomeric Matrix Protein. *Biochemistry* **2009**, *48* (36), 8559−8567.
(42) Hume, J.; Sun, J.; Jacquet, R.; Renfrew, P. D.; Martin, J. A.; Bonneau, R.; Gilchrist, M. L.; Montclare, J. K. Engineered Coiled-Coil Protein Microfibers. *Biomacromolecules* **2014**, *15* (10), 3503−3510.
(43) Hume, J.; Chen, R.; Jacquet, R.; Yang, M.; Montclare, J. K. Tunable Conformation-Dependent Engineered Protein•Gold Nanoparticle Nanocomposites. *Biomacromolecules* **2015**, *16*, 1706−1713.
(44) More, H. T.; Zhang, K. S.; Srivastava, N.; Frezzo, J. A.; Montclare, J. K. Influence of Fluorination on Protein Engineered Coiled-coil Fibers. *Biomacromolecules* **2015**, *16*, 1210−1217.
(45) Haghpanah, J. S.; Yuvienco, C.; Civay, D. E.; Barra, H.; Baker, P. J.; Khapli, S.; Voloshchuk, N.; Gunasekar, S. K.; Muthukumar, M.;


DOI: 10.1021/acs.biomac.8b00158
*Biomacromolecules* 2018, 19, 1614−1624

Montclare, J. K. Artificial Protein Block Copolymers Blocks Comprising Two Distinct Self-Assembling Domains. *ChemBioChem* **2009**, *10* (17), 2733−2735.
(46) Haghpanah, J. S.; Yuvienco, C.; Roth, E. W.; Liang, A.; Tu, R. S.; Montclare, J. K. Supramolecular assembly and small molecule recognition by genetically engineered protein block polymers composed of two SADs. *Mol. BioSyst.* **2010**, *6* (9), 1662−1667.
(47) Dai, M.; Haghpanah, J.; Singh, N.; Roth, E. W.; Liang, A.; Tu, R. S.; Montclare, J. K. Artificial Protein Block Polymer Libraries Bearing Two SADs: Effects of Elastin Domain Repeats. *Biomacromolecules* **2011**, *12* (12), 4240−4246.
(48) Yuvienco, C.; More, H. T.; Haghpanah, J. S.; Tu, R. S.; Montclare, J. K. Modulating Supramolecular Assemblies and Mechanical Properties of Engineered Protein Materials by Fluorinated Amino Acids. *Biomacromolecules* **2012**, *13*, 2273−2278.
(49) Haghpanah, J. S.; Tu, R. S.; Da SIlva, S.; Yan, D.; Mueller, S.; Weder, C.; Foster, E. J.; Gilman, J. W.; Montclare, J. K. Bionanocomposites: Differential Effects of Cellulose Nanocrystals on Protein Diblock Copolymers. *Biomacromolecules* **2013**, *14*, 4360−4367.
(50) DiCesare, P.; Hauser, N.; Lehman, D.; Pasumarti, S.; Paulsson, M. Cartilage oligomeric matrix protein (COMP) is an abundant component of tendon. *FEBS Lett.* **1994**, *354* (2), 237−240.
(51) Hedbom, E.; Antonsson, P.; Hjerpe, A.; Aeschlimann, D.; Paulsson, M.; Rosa-Pimentel, E.; Sommarin, Y.; Wendel, M.; Oldberg, A.; Heinegård, D. Cartilage matrix proteins. An acidic oligomeric protein (COMP) detected only in cartilage. *J. Biol. Chem.* **1992**, *267* (9), 6132−6.
(52) Müller, G.; Michel, A.; Altenburg, E. COMP (Cartilage Oligomeric Matrix Protein) is Synthesized in Ligament, Tendon, Meniscus, and Articular Cartilage. *Connect. Tissue Res.* **1998**, *39* (4), 233−244.
(53) Di Cesare, P. E.; Fang, C.; Leslie, M. P.; Tulli, H.; Perris, R.; Carlson, C. S. Expression of cartilage oligomeric matrix protein (COMP) by embryonic and adult osteoblasts. *J. Orthop. Res.* **2000**, *18* (5), 713−720.
(54) Oldberg, A.; Antonsson, P.; Lindblom, K.; Heinegård, D. COMP (cartilage oligomeric matrix protein) is structurally related to the thrombospondins. *J. Biol. Chem.* **1992**, *267* (31), 22346−50.
(55) Efimov, V. P.; Lustig, A.; Engel, J. The thrombospondin-like chains of cartilage oligomeric matrix protein are assembled by a five-stranded $\alpha$-helical bundle between residues 20 and 83. *FEBS Lett.* **1994**, *341* (1), 54−58.
(56) Efimov, V. P.; Engel, J.; Malashkevich, V. N. Crystallization and preliminary crystallographic study of the pentamerizing domain from cartilage oligomeric matrix protein: a five-stranded $\alpha$-helical bundle. *Proteins: Struct., Funct., Genet.* **1996**, *24* (2), 259−262.
(57) Malashkevich, V. N.; Kammerer, R. A.; Efimov, V. P.; Schulthess, T.; Engel, J. The crystal structure of a five-stranded coiled coil in COMP: a prototype ion channel? *Science* **1996**, *274* (5288), 761−765.
(58) Guo, Y.; Kammerer, R. A.; Engel, J. The unusually stable coiled-coil domain of COMP exhibits cold and heat denaturation in 4−6 M guanidinium chloride. *Biophys. Chem.* **2000**, *85* (2−3), 179−186.
(59) Guo, Y.; Bozic, D.; Malashkevich, V. N.; Kammerer, R. A.; Schulthess, T.; Engel, J. All-trans retinol, vitamin D and other hydrophobic compounds bind in the axial pore of the five-stranded coiled-coil domain of cartilage oligomeric matrix protein. *EMBO J.* **1998**, *17* (18), 5265−5272.
(60) McFarlane, A. A.; Orriss, G.; Okun, N.; Meier, M.; Klonisch, T.; Khajehpour, M.; Stetefeld, J. The Pentameric Channel of COMPcc in Complex with Different Fatty Acids. *PLoS One* **2013**, *8* (5), 0048130.
(61) Prasad, S.; Gupta, S. C.; Tyagi, A. K.; Aggarwal, B. B. Curcumin, a component of golden spice: from bedside to bench and back. *Biotechnol. Adv.* **2014**, *32* (6), 1053−1064.
(62) Gupta, S. C.; Patchva, S.; Aggarwal, B. B. Therapeutic roles of curcumin: lessons learned from clinical trials. *AAPS J.* **2013**, *15* (1), 195−218.
(63) Bansal, S. S.; Goel, M.; Aqil, F.; Vadhanam, M. V.; Gupta, R. C. Advanced Drug-Delivery Systems of Curcumin for Cancer Chemoprevention. *Cancer Prev. Res.* **2011**, *4* (8), 1158−1171.
(64) Studier, F. W. Protein production by auto-induction in high-density shaking cultures. *Protein Expression Purif.* **2005**, *41* (1), 207−234.
(65) Lee, D. L.; Mant, C. T.; Hodges, R. S. A novel method to measure self-association of small amphipathic molecules temperature profiling in reversed-phase chromatography. *J. Biol. Chem.* **2003**, *278* (25), 22918−22927.
(66) Forood, B.; Feliciano, E. J.; Nambiar, K. P. Stabilization of alpha-helical structures in short peptides via end capping. *Proc. Natl. Acad. Sci. U. S. A.* **1993**, *90* (3), 838−842.
(67) Flaugh, S. L.; Mills, I. A.; King, J. Glutamine deamidation destabilizes human $\gamma$D-Crystallin and lowers the kinetic barrier to unfolding. *J. Biol. Chem.* **2006**, *281* (41), 30782−30793.
(68) Rasband, W. S. *ImageJ*; U.S. National Institutes of Health: Bethesda, MD, 1997−2011.
(69) von der Mark, K.; Kirsch, T.; Nerlich, A.; Kuss, A.; Weseloh, G.; Gluckert, K.; Stöss, H. Type X collagen synthesis in human osteoarthritic cartilage. Indication of chondrocyte hypertrophy. *Arthritis Rheum.* **1992**, *35*, 806−811.
(70) Wang, W.; Kirsch, T. Retinoic acid stimulates annexin-mediated growth plate chondrocyte mineralization. *J. Cell Biol.* **2002**, *157* (6), 1061−9.
(71) Viswanadhan, V. N.; Ghose, A. K.; Revankar, G. R.; Robins, R. K. Atomic physicochemical parameters for three dimensional structure directed quantitative structure-activity relationships. 4. Additional parameters for hydrophobic and dispersive interactions and their application for an automated superposition of certain naturally occurring nucleoside antibiotics. *J. Chem. Inf. Model.* **1989**, *29* (3), 163−172.
(72) Klopman, G.; Li, J.-Y.; Wang, S.; Dimayuga, M. Computer Automated log P Calculations Based on an Extended Group Contribution Approach. *J. Chem. Inf. Model.* **1994**, *34* (4), 752−781.
(73) Du Prel, J. B.; Hommel, G.; Röhrig, B.; Blettner, M. Confidence interval or p-value? Part 4 of a series on evaluation of scientific publications. *Dtsch. Arztebl. Int.* **2009**, *106* (19), 335−339.
(74) Dwyer, D. S. Molecular simulation of the effects of alcohols on peptide structure. *Biopolymers* **1999**, *49* (7), 635−645.
(75) Dwyer, D.; Bradley, R. Chemical properties of alcohols and their protein binding sites. *Cell. Mol. Life Sci.* **2000**, *57* (2), 265.
(76) Beck, K.; Gambee, J. E.; Bohan, C. A. The C-terminal domain of cartilage matrix protein assembles into a triple-stranded $\alpha$-helical coiled-coil structure. *J. Mol. Biol.* **1996**, *256* (5), 909−923.
(77) Pace, C. N. Measuring and increasing protein stability. *Trends Biotechnol.* **1990**, *8*, 93−98.
(78) Marky, L. A.; Breslauer, K. J. Calculating thermodynamic data for transitions of any molecularity from equilibrium melting curves. *Biopolymers* **1987**, *26* (9), 1601−1620.
(79) Greenfield, N. J. Using circular dichroism collected as a function of temperature to determine the thermodynamics of protein unfolding and binding interactions. *Nat. Protoc.* **2007**, *1* (6), 2527.
(80) Beck, K.; Gambee, J. E.; Kamawal, A.; Bächinger, H. P. A single amino acid can switch the oligomerization state of the $\alpha$-helical coiled-coil domain of cartilage matrix protein. *EMBO J.* **1997**, *16* (13), 3767−3777.
(81) Krylov, D.; Barchi, J.; Vinson, C. Inter-helical interactions in the leucine zipper coiled coil dimer: pH and salt dependence of coupling energy between charged amino acids. *J. Mol. Biol.* **1998**, *279* (4), 959−972.
(82) Hol, W.; Van Duijnen, P. T.; Berendsen, H. The $\alpha$-helix dipole and the properties of proteins. *Nature* **1978**, *273* (5662), 443.
(83) Manavalan, P.; Ponnuswamy, P. Hydrophobic character of amino acid residues in globular proteins. *Nature* **1978**, *275* (5681), 673−674.
(84) Billinghurst, R. C.; Dahlberg, L.; Ionescu, M.; Reiner, A.; Bourne, R.; Rorabeck, C.; Mitchell, P.; Hambor, J.; Diekmann, O.; Tschesche, H.; Chen, J.; Van Wart, H.; Poole, A. R. Enhanced cleavage


DOI: 10.1021/acs.biomac.8b00158
*Biomacromolecules* 2018, 19, 1614−1624

of type II collagen by collagenases in osteoarthritic articular cartilage. *J. Clin. Invest.* **1997**, *99* (7), 1534−45.
(85) Flannery, C. R.; Little, C. B.; Caterson, B.; Hughes, C. E. Effects of culture conditions and exposure to catabolic stimulators (IL-1 and retinoic acid) on the expression of matrix metalloproteinases (MMPs) and disintegrin metalloproteinases (ADAMs) by articular cartilage chondrocytes. *Matrix Biol.* **1999**, *18* (3), 225−237.
(86) Takishita, Y.; Hiraiwa, K.; Nagayama, M. Effect of retinoic acid on proliferation and differentiation of cultured chondrocytes in terminal differentiation. *J. Biochem.* **1990**, *107* (4), 592−596.
(87) Davies, M. R.; Ribeiro, L. R.; Downey-Jones, M.; Needham, M. R.; Oakley, C.; Wardale, J. Ligands for retinoic acid receptors are elevated in osteoarthritis and may contribute to pathologic processes in the osteoarthritic joint. *Arthritis Rheum.* **2009**, *60* (6), 1722−1732.
(88) Jotanovic, Z.; Mihelic, R.; Sestan, B.; Dembic, Z. Role of interleukin-1 inhibitors in osteoarthritis. *Drugs Aging* **2012**, *29* (5), 343−358.
(89) Stella, V. J.; Rao, V. M.; Zannou, E. A.; Zia, V. Mechanisms of drug release from cyclodextrin complexes. *Adv. Drug Delivery Rev.* **1999**, *36* (1), 3−16.



DOI: 10.1021/acs.biomac.8b00158
*Biomacromolecules* 2018, 19, 1614−1624